Deciphering bacteriophage T5 host recognition Mechanism and infection trigger

Séraphine Degroux, Grégory Effantin, Romain Linares, Guy Schoehn, Cécile Breyton

AMERICAN SOCIETY FOR MICROBIOLOGY | Journal of Virology®

STRUCTURE AND ASSEMBLY

Deciphering Bacteriophage T5 Host Recognition Mechanism and Infection Trigger

Séraphine Degroux,[a] Grégory Effantin,[a] Romain Linares,[a] Guy Schoehn,[a] Cécile Breyton[a]

[a]Université Grenoble Alpes, CNRS, CEA, IBS, Grenoble, France

Séraphine Degroux and Grégory Effantin contributed equally to the work. Author order was determined both alphabetically and in order of increasing seniority.

ABSTRACT Bacteriophages, viruses infecting bacteria, recognize their host with high specificity, binding to either saccharide motifs or proteins of the cell wall of their host. In the majority of bacteriophages, this host recognition is performed by receptor binding proteins (RBPs) located at the extremity of a tail. Interaction between the RBPs and the host is the trigger for bacteriophage infection, but the molecular details of the mechanisms are unknown for most bacteriophages. Here, we present the electron cryomicroscopy (cryo-EM) structure of bacteriophage T5 RBP_{pb5} in complex with its *Escherichia coli* receptor, the iron ferrichrome transporter FhuA. Monomeric RBP_{pb5} is located at the extremity of T5's long flexible tail, and its irreversible binding to FhuA commits T5 to infection. Analysis of the structure of RBP_{pb5} within the complex, comparison with its AlphaFold2-predicted structure, and its fit into a previously determined map of the T5 tail tip in complex with FhuA allow us to propose a mechanism of transmission of the RBP_{pb5} receptor binding to the straight fiber, initiating the cascade of events that commits T5 to DNA ejection.

IMPORTANCE Tailed bacteriophages specifically recognize their bacterial host by interaction of their receptor binding protein(s) (RBPs) with saccharides and/or proteins located at the surface of their prey. This crucial interaction commits the virus to infection, but the molecular details of this mechanism are unknown for the majority of bacteriophages. We determined the structure of bacteriophage T5 RBP_{pb5} in complex with its *E. coli* receptor, FhuA, by cryo-EM. This first structure of an RBP bound to its protein receptor allowed us to propose a mechanism of transmission of host recognition to the rest of the phage, ultimately opening the capsid and perforating the cell wall and, thus, allowing safe channeling of the DNA into the host cytoplasm.

KEYWORDS bacteriophage, electron cryomicroscopy, host recognition, conformational changes

Bacteriophages, bacterial viruses also called phages, are the most abundant and diversified biological entity on Earth (1). As bacterial killers, but also as a means of genetic material exchange, they shape and drive microbial population evolution and diversity (2). The vast majority of phages indexed in databases are composed of a capsid protecting the DNA and a tail, which can be long and contractile (*Myoviridae*), long and flexible (*Siphoviridae*), or short (*Podoviridae*). The tail extremity serves to recognize the host surface and eventually perforate its cell wall and safely channel the DNA from the capsid to the bacterial cytoplasm (3, 4). The distal tip of the tail bears receptor binding proteins (RBPs) that reversibly or irreversibly bind saccharides and/or proteins. Depending on their morphology, RBPs can form fibers (often more than 1,000 residues long and often requiring chaperones to fold) or more globular RBPs, often called tail spike proteins (TSPs) (5). Fibers and TSPs of known structure share an elaborately interwoven, often trimeric state, rich in β-helices. TSPs are multidomain proteins, containing at least a phage

Editor Rebecca Ellis Dutch, University of Kentucky College of Medicine

Address correspondence to Cécile Breyton, Cecile.Breyton@ibs.fr.

The authors declare no conflict of interest.

Received 12 October 2022
Accepted 5 January 2023

binding domain and a receptor binding domain (6). The receptor binding domain can also bear enzymatic activity, digesting the saccharide receptors (5). Because they recognize the bacterial host surface with high specificity and because of their enzymatic activities, phage RBPs can be used to identify bacterial strains for diagnosis (7), to engineer phages with new host ranges (8), or in biotechnology (9). The stoichiometry of RBPs per virion can vary from 1 copy (e.g., RBP_{pb5} in coli-siphophage T5) to 54 (e.g., in lacto-siphophage TP901-1) and maybe more. Phages can also combine RBPs with different binding specificities (10). Multiple binding is proposed to increase the affinity of saccharide binding by avidity. It also has been proposed to position the tail tube correctly for cell wall perforation (11) and has been shown to trigger infection (e.g., in T4 [12, 13] and T7 [14, 15]). All RBP structures determined to date are saccharide binding RBPs, except for the tip of T4's long tail fiber, gp37 (16).

Phage T5, a member of the *Siphoviridae* infecting *E. coli*, is a model phage belonging to the T series introduced in the 1940s (17). It bears an icosahedral capsid that protects the 121-kb DNA and a 250-nm-long flexible tail (18). The host recognition apparatus, consisting of three side tail or L-shaped fibers and a central straight fiber, is located at the distal end of the tail. The central fiber is composed of a trimer of the C-terminal part of the baseplate hub protein (or Tal protein) pb3, followed by a trimer of pb4, at the tip of which is found a monomer of RBP_{pb5}, a 640-residue RBP (4, 19, 20). The side tail fibers, formed by pb1, reversibly bind lipopolysaccharide (LPS) polymannose O antigens O8 and O9 (21, 22), allowing the phage to "walk" at the surface of the bacterium until RBP_{pb5} irreversibly binds to FhuA, an *E. coli* iron-ferrichrome transporter (23). *Shigella* and *Salmonella* strains also bear FhuA proteins, which share high identity with *E. coli* FhuA, and *Salmonella enterica* serovar Paratyphi at least can also be host to T5 (24). T5 side tail fibers can be dispensable under laboratory conditions, as the T5*hd1* mutant that lacks these fibers only impacts host adsorption rates (19, 25), although their modification can also expand the host range (26). Inversely, a point mutation in the RBP_{pb5} gene renders the presence of the side tail fibers indispensable. The RBP_{pb5} gene was thus named *oad*: O antigen dependent (27). *In vitro*, mere interaction of T5 with purified FhuA commits T5 to infection and triggers DNA ejection (28), making T5 an excellent model to study phage-host interaction at the cellular and molecular levels (18, 29). Both RBP_{pb5} and FhuA can be purified and can bind, *in vitro*, in a 1:1, irreversible complex (30, 31). Biophysical analysis of the individual FhuA and RBP_{pb5} proteins compared to the complex showed that some secondary structure changes occur in RBP_{pb5} upon binding to FhuA (31). Also, a low-resolution envelope of the proteins obtained by small-angle neutron scattering (SANS) did not show large conformational changes in either FhuA or RBP_{pb5} upon interaction (32) but did show that RBP_{pb5} is an 8-nm-long elongated protein. We recently solved T5's tail tip structure before and after interaction with FhuA that was reconstituted into a nanodisc and built atomic models for all the tail tip proteins except RBP_{pb5} and FhuA (29). These structures allowed us to describe the sequence of events undertaken by the T5 tail tip upon FhuA-RBP_{pb5} binding, namely, straight fiber bending, opening of the tail tube, its anchoring to the membrane, and finally, formation of a transmembrane channel. Thus, unravelling the structure of RBP_{pb5} before and after interaction with FhuA is the last piece of the puzzle to fully understand the infection trigger mechanism of phage T5 following FhuA binding. This structure is the first one of a nonsaccharide binding RBP bound to its receptor.

RESULTS AND DISCUSSION

Overall structure of the FhuA-RBP_{pb5} complex. The FhuA-RBP_{pb5} complex being so stable and FhuA having been crystallized under different conditions and with different detergents (e.g., references 33 and 34), we tried to crystallize it but obtained only nonreproducible 8-Å anisotropically diffracting crystals (35). To improve the crystals, we produced nanobodies against the complex and used the lanthanide complex XO4 (nucleating and phasing agent) (36) to increase the chances of obtaining well-diffracting crystals. Under neither condition could reproducibly diffracting crystals be obtained. Two-angstrom diffracting

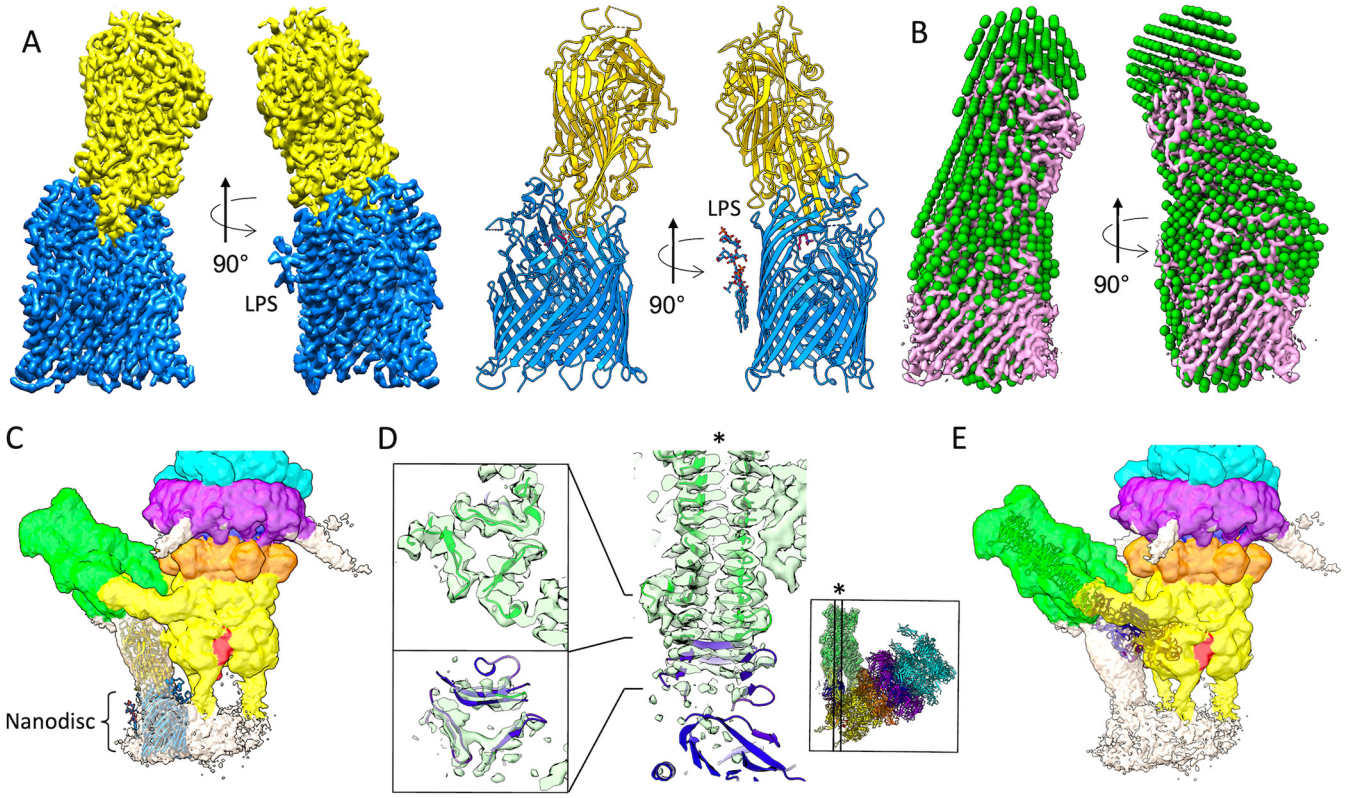

FIG 1 Overall structure of isolated FhuA-RBP$_{pb5}$ and fit in the Tip-FhuA map. (A) Isosurface view of the FhuA-RBP$_{pb5}$ complex in two 90° related side views (left), and ribbon representation of the modeled proteins with FhuA in blue and RBP$_{pb5}$ in gold (right). The LPS density and model is labeled (LPS). (B) FhuA-RBP$_{pb5}$ map fitted into the SANS envelope of FhuA-RBP$_{pb5}$ (32). (C) Isosurface view at high contour level of the unmasked and unfiltered cryo-EM map of T5 Tip-FhuA (EMD-14799) (29) with the structure of FhuA-RBP$_{pb5}$ manually fitted into the empty density below the pb4 spike and anchoring into the nanodisc. Cyan, density corresponding to pb6; purple, p132; orange, pb9; yellow, pb3; green, pb4; red, pb2. Unattributed densities are in white. (D) Manual fit of the AlphaFold2-predicted RBP$_{pb5}$ pb4 binding subdomain into the density-extending pb4 spike, with the pb4 structure shown in ribbon from (EMD-14800, PDB code 7ZN4). Top left, section showing the two last β-strands of the pb4 spike trimer; bottom left, section of the density-extending pb4 spike. The positions of the sections are localized on the longitudinal thin section of the pb4 spike map and model to the right. The position of the latter section is indicated on the Tip-FhuA model by an asterisk in the inset (PDB code 7ZN2). (E) Overall position of the AlphaFold2-predicted RBP$_{pb5}$ structure in the Tip-FhuA map (same as in panel C) after manual fitting of the pb4 binding subdomain as in panel D.

two-dimensional (2-D) crystals were obtained and analyzed in electron diffraction and image analysis in collaboration with Mohamed Chami and Henning Stahlberg (Basel) (35). The crystals were, however, too thick, rendering structure determination impossible. Finally, taking advantage of the "resolution revolution" in electron cryomicroscopy (cryo-EM) (37), we investigated directly the FhuA-RBP$_{pb5}$ structure as a complex in solution by cryo-EM. Even though the complex is relatively small (150 kDa), we obtained a 2.6-Å-resolution three-dimensional (3-D) structure (Fig. 1A; Fig. S1 and Table S1 in the supplemental material).

The complex and RBP$_{pb5}$ within it have an oblong structure, the interaction surface occurring through the distal end of RBP$_{pb5}$, which penetrates into the FhuA barrel down to the FhuA plug. The overall FhuA-RBP$_{pb5}$ structure fits well in the SANS envelope (Fig. 1B) (32). It also fits well in the map of the T5 tail tip interacting with its receptor reconstituted into a nanodisc (Tip-FhuA) (Fig. 1C). In the FhuA-RBP$_{pb5}$ structure, both proteins are very well resolved, except for the FhuA His$_6$ tag located after residue 405 in loop 5 and residues 1 to 17 that contain the FhuA TonB box. These are disordered in all FhuA structures, except when FhuA is crystallized with the TonB C-terminal domain (23, 38). The lipopolysaccharide that copurifies with FhuA could also be fitted. In RBP$_{pb5}$, the first 37 N-terminal residues, as well as residues 333 to 352, 365 to 371, and 427 to 455, could not be traced in the cryo-EM map. These four sequences point to the RBP$_{pb5}$ apex, suggesting, from the fit in the Tip-FhuA map, that they form a phage binding subdomain in interaction with the pb4 spike C terminus. It seems that these loops are therefore unstructured without the pb4 spike partner.

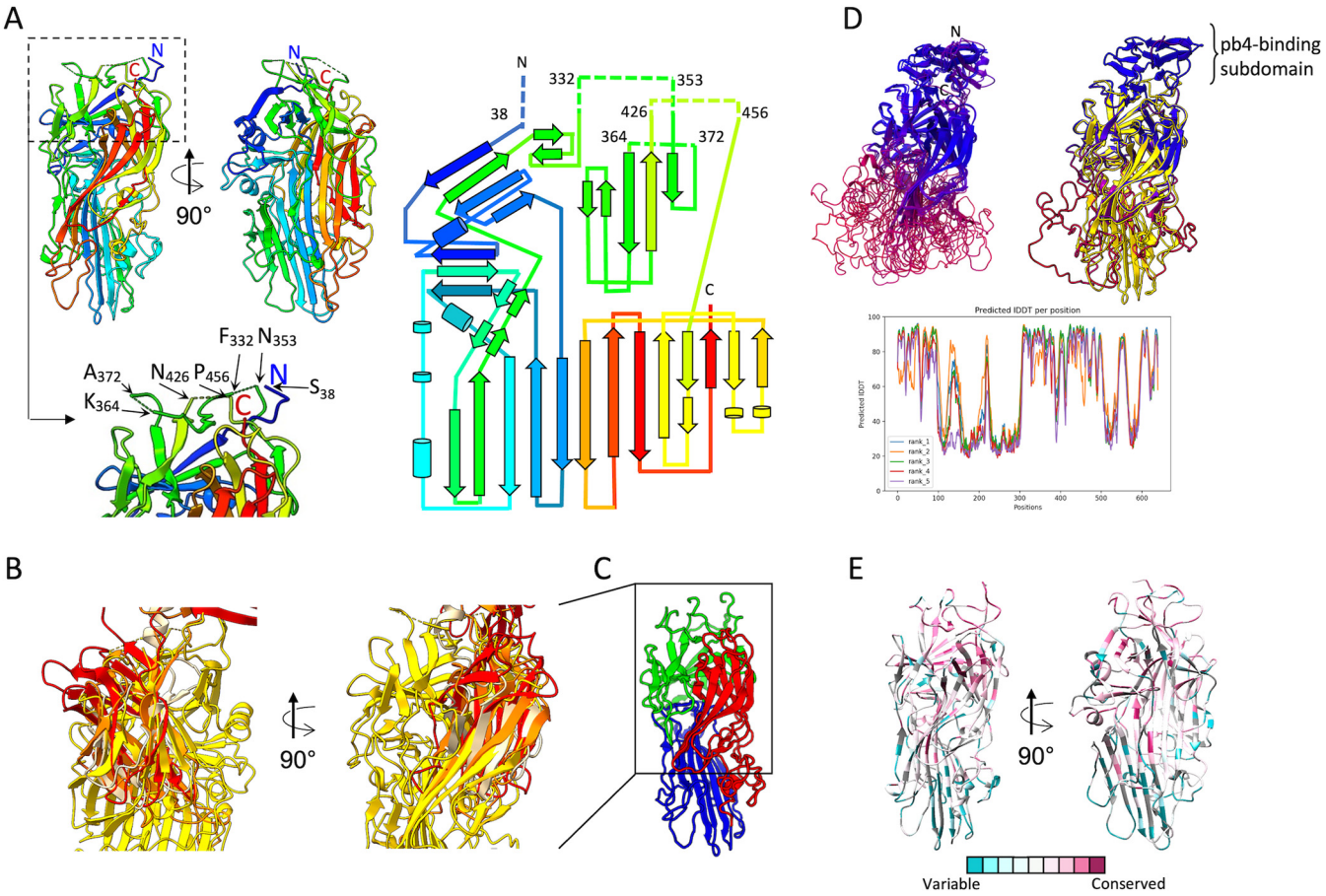

FIG 2 RBP_{pb5} structure analysis. (A) Top left, ribbon representation of RBP_{pb5} structure in the FhuA-RBP_{pb5} complex context in two 90° related side views; right, topology diagram. Both representations are rainbow colored: N-terminal end, blue; C-terminal end, red. Bottom left, blow-up of the apical region of RBP_{pb5} with indication of the residues bounding the unresolved pb4 binding subdomain. (B) DALI alignment of RBP_{pb5} (gold) with domains from phage trimeric proteins with PDB codes 5M9F (orange), 1QEX (red), and 4A0U (beige). (C) Subdomain partitioning proposed by the Sword software (https://www.dsimb.inserm.fr/sword/). The position of the aligned subdomain in panel B is boxed. (D) Top, best ranked AF2-RBP_{pb5} ribbon structure colored by prediction confidence score (high pLDDT, blue; low pLDDT, dark magenta), alone (left) or aligned with the RBP_{pb5} structure within the FhuA-RBP_{pb5} complex (gold) (right). The pb4 binding subdomain, unresolved in our cryo-EM structure, is clearly identified at the apex of AF2-RBP_{pb5}. Bottom, pLDDT scores of the five AF2-RBP_{pb5} predictions. (E) Cryo-EM RBP_{pb5} ribbon representation colored by sequence similarity/divergence (46) (color key as shown) after ClustalO alignment of a BLAST search.

Analysis of the FhuA-RBP_{pb5} structure. (i) RBP_{pb5}. As previously proposed (31), RBP_{pb5} folds as a unique domain rich in β-structures. A large and long central 9-stranded β-sheet serves as the spine of the protein. It is surrounded by shorter β-sheets in the apical half and by random coil loops and small α-helices in the distal half of the protein (Fig. 2A). DALI is a software that searches the Protein Data Bank for structural homologues (39). A DALI analysis does not align the RBP_{pb5} whole structure with any protein of known structure. However, a β-sandwich subdomain shows structural similarity with other proteins: a close analysis of the aligned DALI domains highlights three proteins with the same topology (Fig. 2B). These three matches are all from phage trimeric proteins, two from RBPs (*S. aureus* phage K gp144, PDB code 5M9F, DALI Z-score = 5.1, root mean square deviation [RMSD] 4.4 Å, number of equivalent residues (lali) 100, and phage T7 gp17, PDB code 4A0U, DALI Z-score = 3.2, RMSD 6.6 Å, lali 92) and one from a T4 baseplate protein (gp9, PDB code 1QEX, DALI Z-score = 4.9, RMSD 4.9 Å, lali 87, with, however, a slight topological difference on the last β-strand). In RBP_{pb5}, the β-strands are longer. This domain displays an original fold, which is nevertheless similar to the knob domain of other viral RBPs, that is believed to interact with the host receptor (40). This again illustrates the "Lego" strategy of phages and viruses, which use and exchange functional modules (41). The Sword software

analyses a protein structure and proposes domain partitioning. It proposes that RBP_{pb5} folds as a unique domain; as an alternative, the algorithm also proposes subdivision of RBP_{pb5} into three subdomains, including the common RBP subdomain (Fig. 2C).

Structure prediction software programs have made tremendous progress over the last few years (42), AlphaFold2 in particular (43). We submitted the RBP_{pb5} sequence to AlphaFold2 to investigate the structure of RBP_{pb5} missing the phage binding subdomain and, also, to compare an RBP_{pb5} predicted structure with our structure of RBP_{pb5} in complex with FhuA. We obtained five different predicted models (AF2-RBP_{pb5}) (Fig. 2D; the PDB file of the best predicted model is given in the supplemental material). For all models, the AF2-RBP_{pb5} structure can be divided into two halves: the distal half is predicted with a poor confidence (predicted local-distance difference test [pLDDT] $<$ 50), while the apical half is predicted with high confidence (pLDDT $>$ 70). This includes the N terminus and disordered loops of our RBP_{pb5} structure, which are predicted to form a small β-helix, attached to the RBP_{pb5} core by five linkers (residues 37 to 45, 327 to 336, 353 to 357, 426 to 432, and 456 to 463). This β-helix would perfectly extend the pb4 spike: indeed, it fits very well in the density present in the Tip-FhuA cryo-EM map extending the pb4 β-helix (Fig. 1D). However, the core domain of AF2-RBP_{pb5} does not fit at all the rest of the low-resolution density available for RBP_{pb5} (Fig. 1E). Indeed, our Tip-FhuA map rather suggests a different angle between the pb4 binding subdomain and the RBP_{pb5} core domain, made possible by the flexibility given by the five linkers (see also below). This flexibility, visible on negative stain images (see Fig. 5 in reference 20) explains in part why cryo-EM image analysis of the T5 tip and Tip-FhuA did not generate a high-resolution map for RBP_{pb5}.

Considering the predicted structure of the AF2-RBP_{pb5} core domain, the apical half aligns very well with our RBP_{pb5} structure (RMSD ranging from 0.811 to 0.979 Å over 222 to 291 residues depending on the AF2 model). This is coherent with the good level of confidence calculated by AlphaFold2. On the other hand, alignment of the poorly predicted distal half, corresponding to the FhuA binding domain, is rather bad (overall RMSD ranging from 7.6 to 18.2 Å over all 572 residues for the five AF2-RBP_{pb5} models). pLDDT values below 50 are indicated to be strong predictors of disorder (44), suggesting that the regions are unstructured under physiological conditions: they would only fold upon interaction with FhuA. Even though AlphaFold predictions are not always correct, disorder in the RBP_{pb5} distal half is consistent with biophysical and biochemical data that allow the conclusion that isolated RBP_{pb5} is less structured and sees an increase in its β-sheet content at the expense of other structures, as well as a rigidification of its tertiary structure, upon binding to FhuA (31). This also explains the strong thermal stabilization of RBP_{pb5} upon binding to FhuA (melting temperature [T_m] = 43°C for RBP_{pb5} alone and 89°C for FhuA-RBP_{pb5}) (31). We also submitted the FhuA-RBP_{pb5} complex to AlphaFold-Multimer (45): the prediction exhibits a wrong orientation between FhuA and RBP_{pb5} and a very small interacting surface. RBP_{pb5} does, however, appear a bit more structured, in particular its large central sheet (Fig. S1F). We have proposed the FhuA-RBP_{pb5} complex to CASP15 and are expecting the results by the end of 2022.

Whereas there are no RBP_{pb5} homologues in the PDB, a BLAST search finds a large number of proteins ($>$100), with identities ranging from 29.0 to 96.3%. They are described as *E. coli*, *Salmonella*, *Shigella*, or *Klebsiella* phage hypothetical RBPs or RBPs. This is consistent with the fact that the T5-like genus is well represented in the databases. Clustal alignment and the ConSurf Server (46) allow visualization of the distribution of conserved versus variable residues on the RBP_{pb5} structure (Fig. 2E). The dichotomy of the distribution is quite striking: the apical half of RBP_{pb5} is largely conserved, `in particular for the unresolved N terminus and loops (not shown), while the distal half is much more variable. This trend—phage binding domain conserved/receptor binding domain much more variable—is quite general in RBPs, fibers, and TSPs, highlighting that the receptor binding domains are under heavy evolutionary pressure to diversify as they interact with a

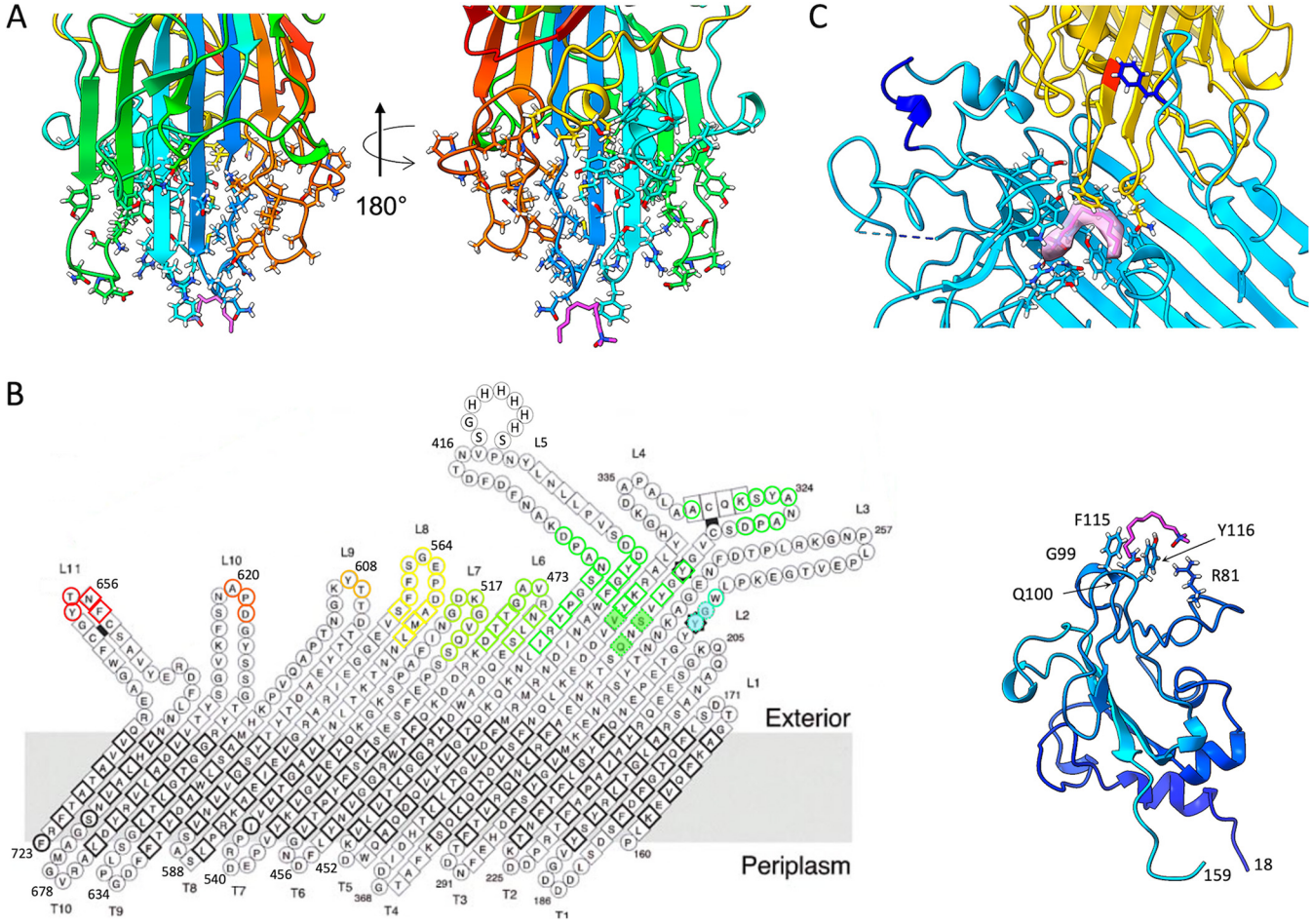

FIG 3 Surface of interaction between FhuA and RBP_{pb5}. (A) Two orientations of a rainbow-colored ribbon representation of RBP_{pb5}'s distal part, with residues involved in the interactions, as determined by PISA, shown in sticks. The $C_{10}DAO$ molecule is shown in pink. (B) Left, topology diagram of FhuA barrel (from reference 33), on which are indicated the residues involved in the interaction (dotted-line and filled symbols indicate residues interacting exclusively with the $C_{10}DAO$ molecule). Right, ribbon diagram of FhuA plug, with residues involved in the interactions and the $C_{10}DAO$ molecule shown in sticks. (C) Zoomed image of the FhuA-RBP_{pb5} interface. FhuA is in cyan and RBP_{pb5} in gold. Both proteins are in ribbon form, with the residues involved in $C_{10}DAO$ binding in sticks. The $C_{10}DAO$ density is shown in pink. FhuA PADKGH is highlighted in blue. In RBP_{pb5}, G166 is highlighted in orange and FhuA-F566 in blue sticks.

large variety of host targets, while the phage binding domain, bearing a structural function, is more constrained by interaction with its phage partner(s) (47).

(ii) FhuA. The structure of FhuA has been solved in its apo form, in complex with many ligands and with the C-terminal domain of TonB (23). The different structures are remarkably similar, with RMSDs between the 11 different structures below 1.93 Å over all 696 common residues. The main difference between the different structures is the N-terminal region: in FhuA apo structures, residues 19 to 30 are structured as an α-helix, whereas in structures binding TonB-dependent ligands, a conformation that is superimposable to the TonB-bound conformation is adopted (23). In agreement with the fact that T5 infection is TonB independent, the conformation of RBP_{pb5}-bound FhuA residues 19 to 30 is that of apo FhuA.

FhuA-RBP_{pb5} interface. RBP_{pb5} interaction with FhuA occurs through the distal β-turns and loops of the central sheet and through random coil loops and small α-helices in the distal half of RBP_{pb5}, with a total of 63 residues involved, as calculated by PISA, a software that analyses interfaces from PDB files (Fig. 3A) (48). In FhuA, interactions are mediated by the apical tip of the plug, including residues in loops 4 to 11 and in β-strands 7 to 12, with a total of 64 residues involved (Fig. 3B). The surface of interaction is large, with a buried area of 2,034 $Å^2$ and a PISA calculated energy of -21.4 kcal/mol, and the interaction is stabilized by 13 hydrogen bonds and hydrophobic interactions, explaining the

quasi-irreversibility of the interaction (31). Interestingly, a C_{10}DAO (*n*-decyl *N*,*N*-dimethylamine *N*-oxide) molecule, contained in the buffer, could be modeled at the interface between the FhuA plug and RBP_{pb5} (Fig. 3C; Fig. S1E). It overlapped the ferrichrome hydrophobic binding pocket and interacted, on the FhuA side, with 13 residues—four from the plug, four from loops 3 and 4, and five from β-strands 7 to 9, with a hydrogen bond between Y116 and the carboxyl of the amine oxide head group. The C_{10}DAO binding pocket is further completed by four residues from loops of the tip of the RBP_{pb5} β-sheet, further stabilizing the interaction between the two proteins (Fig. 3C).

T5 is a historic phage and a prototype of the siphophages, for which host binding has been extensively studied in the past. The presence of an RBP binding to FhuA was proposed while studying the *oad* mutant, which had a reduced affinity to FhuA (19, 27). Later, Mondigler et al. identified the *oad* mutation: Gly166 is switched to a Trp (49). In our structure, Gly166 participates in the binding interface, making a C-H. . .Π interaction with FhuA Phe566 (Fig. 3C). A Gly→Trp mutation would thus indeed destabilize the protein-protein interaction interface. Mondigler et al. also investigated the ability of different RBP_{pb5} large-deletion (over 40 residues) and insertion mutants to bind to FhuA (49). Apart from one (deletion of the 153 C-terminal residues), none retained binding abilities, which is explained by the tight fold of FhuA-bound RBP_{pb5}.

FhuA's binding to RBP_{pb5} has also been studied from the FhuA perspective: before the FhuA structure was known, Killmann et al. investigated T5 binding loops in FhuA by competitive peptide mapping (50). They identified a peptide—$_{334}$PADKGH$_{339}$—of FhuA loop 4 that induced DNA ejection when incubated with T5, in a temperature-dependent manner. However, we could not reproduce the results with a slightly longer peptide (APADKGHY), and, as seen in our structure, this sequence does not appear to be involved in RBP_{pb5} binding (Fig. 3C). Single substitutions impairing T5 binding could not be isolated unless they perturbed FhuA's overall structure (23), and deletion of loops 3 to 11, except for loop 8, did not prevent T5 binding (51). This can be explained by the large interacting surface between the two proteins, which could compensate single substitutions or loop deletions. There does not seem to be a structural rationale for loop 8 being more important for RBP_{pb5} binding than other loops. Deletion of loop 8 also impairs T1 and ϕ80 binding and ferrichrome transport, suggesting that its deletion might prevent the proper folding of FhuA. A FhuA plugless mutant was also investigated for its ability to bind T5: an *E. coli* strain with deletion of endogenous FhuA and expressing FhuAΔplug was resistant to T5, thus suggesting that RBP_{pb5} did not bind to FhuAΔplug (52). Given the surface of interaction provided by the FhuA barrel loops, this result suggests that the latter are either flexible or adopt a different conformation in FhuAΔplug than in wild-type (WT) FhuA, preventing RBP_{pb5} binding. Indeed, the plug does not provide a larger surface of interaction than individual FhuA barrel loops. The role of the plug is, however, important in the overall stabilization of the interaction between FhuA and RBP_{pb5}, as previously suggested (31): whereas FhuA displays two T_ms, one for the plug (64°C) and one for the barrel (75°C), the RBP_{pb5}-FhuA complex displays a unique T_m that is shifted to 89°C.

T5 is described as infecting *E. coli*; however, some other strains also bear FhuA. Thus, we tested T5's sensitivity on different *E. coli*, *Shigella*, and *Salmonella* strains, which were chosen because of their different levels of FhuA identity with the FhuA of the *E. coli* laboratory strain, ranging from 96% to 100% (Fig. S2). T5 sensitivity tests were performed in the presence of dipyridyl, an iron chelator that boosts FhuA expression. Surprisingly, only *Salmonella bongori* was sensitive to T5. The FhuA sequence alignment, however, shows some differences in the residues interacting with RBP_{pb5}, presumably reflecting the resilience of the FhuA-RBP_{pb5} interaction. We checked for T5 irreversible adsorption on all strains, but only *Salmonella bongori* showed adsorption, comparable to that of *E. coli*. Interestingly, enteropathogenic *E. coli* (EPEC) and the *Shigella* strains were resistant to T5 despite there being no difference in the interacting residues (Fig. S2). Resistance to T5 may be explained by a different O antigen content of the LPS molecules, FhuA being blocked by a superinfection exclusion protein coded

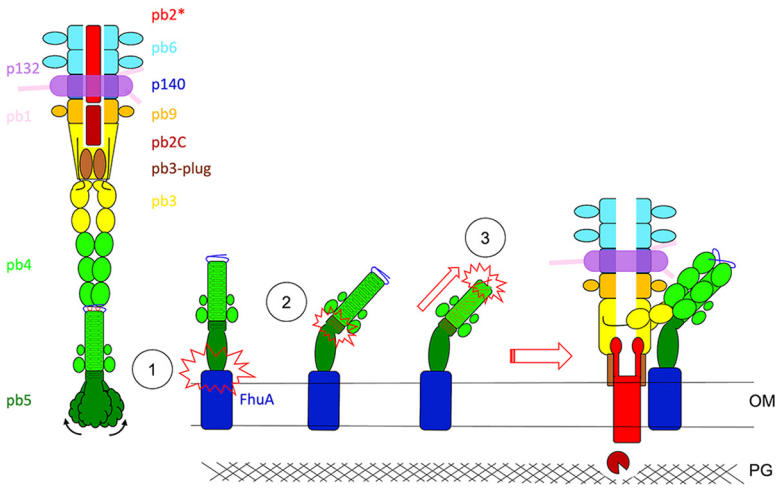

FIG 4 Proposed mechanism of signal transduction of FhuA's binding to the pb4 spike through RBP_{pb5}. Left, within the T5 tail, the RBP_{pb5} distal half is unstructured and the RBP_{pb5} core is flexible with respect to the pb4 binding subdomain. Upon binding to FhuA, the RBP_{pb5} distal half gets structured (1). This would induce rigidification of the whole protein, in particular of the linkers between the core of RBP_{pb5} and the pb4 binding subdomain, which are stabilized at an angle of ~45° (2). This in turn would induce a modification of the twist of the pb4 β-helix (3), which induces the opening of the tail tube, its anchoring to the membrane, the expulsion of the tape measure protein, and the formation of a channel across the host outer membrane (29).

by a prophage in their genomes, or by the synthesis of a capsule, shielding FhuA from the phage.

Conclusion. We present here the first structure of an RBP, RBP_{pb5}, in complex with its protein receptor, FhuA. Analysis of this structure compared to that predicted for RBP_{pb5} and fitted into the T5 tail tip map after interaction with FhuA (Tip-FhuA) (29) allows us to propose a mechanism that would transmit FhuA binding to pb4 through RBP_{pb5} (Fig. 4): the apical subdomain of AF2-RBP_{pb5} shows a small structured β-helix that fits well in our Tip-FhuA map, in the densities extending the pb4 β-helix spike. This RBP_{pb5} subdomain would serve as an adaptor between the trimeric pb4 and the monomeric RBP_{pb5}. The presence of linkers between this subdomain and the RBP_{pb5} core confers flexibility between these two parts of the protein. The AF2-RBP_{pb5} predicted structure and biophysical analysis of RBP_{pb5} (31) suggest that the distal half of RBP_{pb5} is unstructured when not bound to FhuA. Upon binding to FhuA, RBP_{pb5}'s distal half becomes structured, rigidifying the protein. In our Tip-FhuA map, the RBP_{pb5} core and the pb4 binding subdomain lie at an angle of ~45°. We suggest that rigidification of the RBP_{pb5} distal half is transmitted to the pb4 binding subdomain, where it imposes a ~45° kink. This would constrain the RBP_{pb5} pb4 binding subdomain, which in turn would constrain the pb4 β-helix spike and induce the different twist in the pb4 β-helix. This last twist could then initiate the conformational change cascade that results in the tail tube opening and the tube anchoring to the membrane in register with a channel that goes through the outer membrane (29). Definite confirmation of this hypothesis will require determination of the structure of pb4-bound RBP_{pb5} before and after interaction with FhuA.

MATERIALS AND METHODS

Bacterial and phage strains. The heat-stable deletion mutant T5st0 was used for sensitivity and adsorption tests. *E. coli* strain F, a fast-adsorbing strain for T5, was used for the production of T5st0 and for control of free T5 in adsorption tests. *Shigella flexneri* (CIP 106171), *Shigella sonnei* (CIP 106204), *Salmonella enterica* serovar Typhimurium (CIP 104474), *Salmonella enterica* serovar Indica (CIP 102501T), *Salmonella bongori* (CIP 82.33T), and enteropathogenic *E. coli* (CIP 52.170) were used for T5 sensitivity and adsorption tests. *E. coli* strains AW740 and BL21(DE3) were used for FhuA and RBP_{pb5} expression, respectively.

FhuA and RBP_{pb5} production and purification. FhuA was purified from *E. coli* strain AW740 transformed with a plasmid encoding the complete *fhuA* gene, including its signal sequence, and in which a His-tag coding sequence has been inserted in extracellular loop L5. A His tag in this position was shown not to impair RBP_{pb5} binding (30). RBP_{pb5} was purified from *E. coli* strain BL21(DE3) carrying the *oad* gene

encoding RBP_{pb5} fused to a His tag-coding sequence 3′ from *oad* in a pET-28 vector (30). Cells were grown in LB medium at 37°C in the presence of the iron-chelating agent dipyridine (100 μM) for AW740 cells and at 20°C without induction for BL21(DE3) cells. FhuA and RBP_{pb5} purifications were carried out as described previously (31). The FhuA-RBP_{pb5} complex was formed by adding equimolar amounts of the two proteins, which results in 100% complex formation as described in reference 30. Detergent exchange on the FhuA-RBP_{pb5} complex was performed by a 10-times dilution in deionized water and centrifugation at 100,000 $\times$ *g* for 45 min at 4°C. The pellet was rinsed with water and resuspended in 20 mM Tris, 1.6% C_{10}DAO at a protein concentration of 4.3 mg/mL.

Cryo-EM sample preparation. Typically, 3.5 μL of the FhuA-RBP_{pb5} complex was deposited on a freshly glow-discharged (25 mA, 30 s) Cu/Rh 400-mesh Quantifoil R 2/1 EM grid and flash-frozen in nitrogen-cooled liquid ethane using a ThermoFisher Mark IV Vitrobot device (100% humidity, 20°C, 2 s blotting time, blot force 1). Preliminary screening of freezing conditions was performed on an FEI F20 electron microscope.

Two different data sets were acquired on the same grid. For both data sets, 60-frame movies with a total dose of 60 $e^-/Å^2$ were acquired on a ThermoFisher Scientific Titan Krios G3 transmission electron microscope (European Synchrotron Radiation Facility, Grenoble, France) (53) operated at 300 kV and equipped with a Gatan Quantum LS/967 energy filter (slit width of 20 eV used) coupled to a Gatan K2 summit direct electron detector. Automated data collection was performed using ThermoFisher Scientific EPU software. A nominal magnification of $\times$130,000 was used, resulting in a calibrated pixel size at the specimen level of 1.052 Å/pixel. For the first data set, 777 movies were acquired with a phase plate, close to focus (between -0.5 and -1.0 μm), while for the second data set, 8,752 movies were acquired without a phase plate and with a defocus ranging between -1.2 and -2.6 μm.

EM image processing. For both data sets, the processing was done with Relion (54). Motion correction using 5-by-5 patches was done with Motioncor2 (55), while contrast transfer function (CTF) estimation was done with Gctf (56).

For Data Set S1, an initial set of particles was selected with the Laplacian of Gaussian (LoG) picker in Relion. After 2-D classification with 2-times-binned particles, nicely defined 2-D classes were used as references for a template-based picking. Following another 2-D classification, an initial model was obtained in Relion, which was then used to get a first 3-D reconstruction. 3-D classification (without a mask) was performed to select the best particles, which were then used to compute a final 3-D reconstruction at 6.7 Å (at a Fourier shell correlation [FSC] of 0.143) into which the atomic model of FhuA (PDB code 1QFG) could be unambiguously fitted (not shown).

For Data Set S2, 2-D projections of the 3-D model obtained from Data Set S1 were used as a template to automatically pick all micrographs. In all, 2,191,586 particles were obtained, binned two times and further subjected to two rounds of 2-D classification to remove obvious outliers. A first 3-D classification was done without any mask, and the selected particles were re-extracted without binning. Following a 3-D refinement step, two successive 3-D classifications with a mask following the contour of the complex were performed without any image alignment, leading to a homogenous subset of 109,350 particles. Then, particle polishing and two rounds of CTF refinements (magnification anisotropy, beam tilt, and per-particle defocus) were performed before a last 3-D refinement yielded the final 3-D reconstruction at 2.6-Å average resolution (at an FSC of 0.143). The final map was sharpened using DeepEMhancer (57).

Model building. The RBP_{pb5} protein model was built *de novo* in a FhuA-RBP_{pb5} cryo-EM map using Coot (version 0.9.2) (58). FhuA was adapted from an FhuA structure solved by X-ray crystallography (PDB code 2GRX). The two individual proteins and the complex were then refined using the PHENIX (version 1.18.2-3874) Real Space Refine tool (58). Structure validation was done using the MolProbity online tool.

AlphaFold structure prediction. AlphaFold prediction of RBP_{pb5} was performed on the CollabFold server with AlphaFold2 version 1.3 (59). AlphaFold prediction of FhuA-RBP_{pb5} was performed using AlphaFoldMultimer (45).

Phage sensitivity tests. *Shigella*, *Salmonella*, and *E. coli* strains were grown in LB medium at 37°C, 180 rpm until reaching an optical density at 600 nm (OD_{600}) of 0.5. Amounts of 1.2 mL of LB soft agar were inoculated with 300 μL of culture and spread on an LB petri dish. Serial dilutions of phage T5, at 0 to 10^9 PFU/mL, were directly spotted on the soft agar. The titer was estimated by counting lysis plaques in the spotted area after overnight incubation at 37°C.

Irreversible phage adsorption tests. To 5 mL of each strain grown in LB medium at an OD_{600} of 0.2, 0.01 M $CaCl_2$, 0.04 M $MgCl_2$, and T5 at a multiplicity of infection of 0.5 were added, and the mixtures incubated at 37°C. Amounts of 200 μL of infected cells were collected at different times, vigorously vortexed for 10 s, and centrifuged for 10 min at 15,000 $\times$ *g*. The supernatants containing free phage (unabsorbed and reversibly bound particles) were titrated on *E. coli* strain F using the double-layer agar method described above.

Data availability. Cryo-EM density maps of FhuA-RBP_{pb5} and the associated atomic coordinates have been deposited in the Electron Microscopy Data Bank (EMDB) and in the Protein Data Bank (PDB) under the following accession numbers: PDB code 8B14 and EMD-15802.

SUPPLEMENTAL MATERIAL

Supplemental material is available online only.

SUPPLEMENTAL FILE 1, PDF file, 2.6 MB.

SUPPLEMENTAL FILE 2, PDF file, 0.4 MB.

ACKNOWLEDGMENTS

We acknowledge the thesis work of Ali Flayhan for efforts in the 2-D and 3-D crystallization of the FhuA-RBP_{pb5} complex and the shorter or longer internship work of Flavien Grégoire, Charles-Adrien Arnaud, Marie-Ange Marrel, Sarra Landri, Emmi Mikkola, and Annelise Vermot, who tried to optimize the RBP_{pb5} construct or crystallize the complex with nanobodies, and Edine Hammouche, who performed some T5 adsorption tests. We also acknowledge Mohamed Chami and Henning Stahlberg (Biozentrum, Basel) for the 2-D crystal adventure and Alain Roussel and Aline Desmyter (Marseille, https://nabgen.org/) for production of nanobodies directed against the FhuA-RBP_{pb5} complex. We thank Eric Faudry for the kind gift of the *Salmonella enterica* serovar Typhimurium, *Shigella flexneri*, and *E. coli* EPEC strains, Daphna Fenel for quality control by negative staining, Emmanuelle Neumann for help with the F20 electron microscope, and Martin Blackledge for English editing of the text.

This research was funded by the Agence Nationale de la Recherche, grants number ANR-16-CE11-0027 and ANR-21-CE11-0023 to G.S. and C.B.

This research used the EM facility at the Grenoble Instruct-ERIC Center (ISBG; UAR 3518 CNRS-CEA-UGA-EMBL) within the Grenoble Partnership for Structural Biology (PSB). IBS platform access was supported by FRISBI (ANR-10-INBS-05-02) and GRAL, a project of the University Grenoble Alpes graduate school (Ecoles Universitaires de Recherche), CBH-EUR-GS (ANR-17-EURE-0003). The electron microscope facility is supported by the Auvergne-Rhône-Alpes Region, the Fondation pour la Recherche Médicale (FRM), the Fonds FEDER, and the GIS-Infrastructures en Biologie Santé et Agronomie (IBiSA). We acknowledge the provision of in-house experimental time from the CM01 facility at the ESRF. IBS acknowledges integration into the Interdisciplinary Research Institute of Grenoble (IRIG, CEA).

We declare no conflict of interest.

C.B. conceived the project. S.D. prepared the FhuA-RBP_{pb5} complex. G.S. and R.L. optimized cryogrid preparation. G.E. recorded and processed the cryo-EM data. S.D. performed T5 sensitivity and adsorption experiments and built the atomic model with help from R.L. C.B. analyzed and interpreted the structure. C.B. wrote the paper with contributions from G.E., G.S., and S.D. All authors contributed to the editing of the manuscript.

REFERENCES

1. Dion MB, Oechslin F, Moineau S. 2020. Phage diversity, genomics and phylogeny. Nat Rev Microbiol 18:125–138. https://doi.org/10.1038/s41579-019-0311-5.
2. Suttle CA. 2007. Marine viruses—major players in the global ecosystem. Nat Rev Microbiol 5:801–812. https://doi.org/10.1038/nrmicro1750.
3. Nobrega FL, Vlot M, de Jonge PA, Dreesens LL, Beaumont HJE, Lavigne R, Dutilh BE, Brouns SJJ. 2018. Targeting mechanisms of tailed bacteriophages. Nat Rev Microbiol 16:760–773. https://doi.org/10.1038/s41579-018-0070-8.
4. Linares R, Arnaud C-A, Degroux S, Schoehn G, Breyton C. 2020. Structure, function and assembly of the long, flexible tail of siphophages. Curr Opin Virol 45:34–42. https://doi.org/10.1016/j.coviro.2020.06.010.
5. Broeker NK, Barbirz S. 2017. Not a barrier but a key: how bacteriophages exploit host's O-antigen as an essential receptor to initiate infection. Mol Microbiol 105:353–357. https://doi.org/10.1111/mmi.13729.
6. Goulet A, Spinelli S, Mahony J, Cambillau C. 2020. Conserved and diverse traits of adhesion devices from Siphoviridae recognizing proteinaceous or saccharidic receptors. Viruses 12:512. https://doi.org/10.3390/v12050512.
7. Filik K, Szermer-Olearnik B, Oleksy S, Brykała J, Brzozowska E. 2022. Bacteriophage tail proteins as a tool for bacterial pathogen recognition—a literature review. Antibiotics (Basel) 11:555. https://doi.org/10.3390/antibiotics11050555.
8. Dams D, Brøndsted L, Drulis-Kawa Z, Briers Y. 2019. Engineering of receptor-binding proteins in bacteriophages and phage tail-like bacteriocins. Biochem Soc Trans 47:449–460. https://doi.org/10.1042/BST20180172.
9. Santos SB, Costa AR, Carvalho C, Nóbrega FL, Azeredo J. 2018. Exploiting bacteriophage proteomes: the hidden biotechnological potential. Trends Biotechnol 36:966–984. https://doi.org/10.1016/j.tibtech.2018.04.006.
10. Sørensen AN, Woudstra C, Sørensen MCH, Brøndsted L. 2021. Subtypes of tail spike proteins predicts the host range of Ackermannviridae phages. Comput Struct Biotechnol J 19:4854–4867. https://doi.org/10.1016/j.csbj.2021.08.030.
11. Taylor NMI, van Raaij MJ, Leiman PG. 2018. Contractile injection systems of bacteriophages and related systems. Mol Microbiol 108:6–15. https://doi.org/10.1111/mmi.13921.
12. Hu B, Margolin W, Molineux IJ, Liu J. 2015. Structural remodeling of bacteriophage T4 and host membranes during infection initiation. Proc Natl Acad Sci U S A 112:E4919–E4928. https://doi.org/10.1073/pnas.1501064112.
13. Yap ML, Klose T, Arisaka F, Speir JA, Veesler D, Fokine A, Rossmann MG. 2016. Role of bacteriophage T4 baseplate in regulating assembly and infection. Proc Natl Acad Sci U S A 113:2654–2659. https://doi.org/10.1073/pnas.1601654113.
14. Hu B, Margolin W, Molineux IJ, Liu J. 2013. The bacteriophage T7 virion undergoes extensive structural remodeling during infection. Science 339:576–579. https://doi.org/10.1126/science.1231887.
15. González-García VA, Pulido-Cid M, Garcia-Doval C, Bocanegra R, van Raaij MJ, Martín-Benito J, Cuervo A, Carrascosa JL. 2015. Conformational changes leading to T7 DNA delivery upon interaction with the bacterial receptor. J Biol Chem 290:10038–10044. https://doi.org/10.1074/jbc.M114.614222.
16. Bartual SG, Otero JM, Garcia-Doval C, Llamas-Saiz AL, Kahn R, Fox GC, van Raaij MJ. 2010. Structure of the bacteriophage T4 long tail fiber receptor-binding tip. Proc Natl Acad Sci U S A 107:20287–20292. https://doi.org/10.1073/pnas.1011218107.
17. Demerec M, Fano U. 1945. Bacteriophage-resistant mutants in Escherichia coli. Genetics 30:119–136. https://doi.org/10.1093/genetics/30.2.119.

18. Arnaud C-A, Effantin G, Vivès C, Engilberge S, Bacia M, Boulanger P, Girard E, Schoehn G, Breyton C. 2017. Bacteriophage T5 tail tube structure suggests a trigger mechanism for Siphoviridae DNA ejection. Nat Commun 8:1953. https://doi.org/10.1038/s41467-017-02049-3.
19. Heller KJ, Bryniok D. 1984. O antigen-dependent mutant of bacteriophage T5. J Virol 49:20–25. https://doi.org/10.1128/JVI.49.1.20-25.1984.
20. Zivanovic Y, Confalonieri F, Ponchon L, Lurz R, Chami M, Flayhan A, Renouard M, Huet A, Decottignies P, Davidson AR, Breyton C, Boulanger P. 2014. Insights into bacteriophage T5 structure from analysis of its morphogenesis genes and protein components. J Virol 88:1162–1174. https://doi.org/10.1128/JVI.02262-13.
21. Heller K, Braun V. 1982. Polymannose O-antigens of Escherichia coli, the binding sites for the reversible adsorption of bacteriophage T5+ via the L-shaped tail fibers. J Virol 41:222–227. https://doi.org/10.1128/JVI.41.1.222-227.1982.
22. Garcia-Doval C, Castón JR, Luque D, Granell M, Otero JM, Llamas-Saiz AL, Renouard M, Boulanger P, van Raaij MJ. 2015. Structure of the receptor-binding carboxy-terminal domain of the bacteriophage T5 L-shaped tail fibre with and without its intra-molecular chaperone. Viruses 7:6424–6440. https://doi.org/10.3390/v7122946.
23. Braun V. 2009. FhuA (TonA), the career of a protein. J Bacteriol 191:3431–3436. https://doi.org/10.1128/JB.00106-09.
24. Graham AC, Stocker BA. 1977. Genetics of sensitivity of Salmonella species to colicin M and bacteriophages T5, T1, and ES18. J Bacteriol 130:1214–1223. https://doi.org/10.1128/jb.130.3.1214-1223.1977.
25. Saigo K. 1978. Isolation of high-density mutants and identification of nonessential structural proteins in bacteriophage T5; dispensability of L-shaped tail fibers and a secondary major head protein. Virology 85:422–433. https://doi.org/10.1016/0042-6822(78)90449-X.
26. Zhang J, Ning H, Lin H, She J, Wang L, Jing Y, Wang J. 2022. Expansion of the plaquing host range and improvement of the absorption rate of a T5-like Salmonella phage by altering the long tail fibers. Appl Environ Microbiol 88:e00895-22. https://doi.org/10.1128/aem.00895-22.
27. Krauel V, Heller KJ. 1991. Cloning, sequencing, and recombinational analysis with bacteriophage BF23 of the bacteriophage T5 oad gene encoding the receptor-binding protein. J Bacteriol 173:1287–1297. https://doi.org/10.1128/jb.173.3.1287-1297.1991.
28. Boulanger P, Le Maire M, Bonhivers M, Dubois S, Desmadril M, Letellier L. 1996. Purification and structural and functional characterization of FhuA, a transporter of the Escherichia coli outer membrane. Biochemistry 35:14216–14224. https://doi.org/10.1021/bi9608673.
29. Linares R, Arnaud C-A, Effantin G, Darnault C, Epalle NH, Erba EB, Schoehn G, Breyton C. 2022. Structural basis of bacteriophage T5 infection trigger and E. coli cell wall perforation. bioRxiv. https://doi.org/10.1101/2022.09.20.507954.
30. Plançon L, Janmot C, Le Maire M, Desmadril M, Bonhivers M, Letellier L, Boulanger P. 2002. Characterization of a high-affinity complex between the bacterial outer membrane protein FhuA and the phage T5 protein pb5. J Mol Biol 318:557–569. https://doi.org/10.1016/S0022-2836(02)00089-X.
31. Flayhan A, Wien F, Paternostre M, Boulanger P, Breyton C. 2012. New insights into pb5, the receptor binding protein of bacteriophage T5, and its interaction with its Escherichia coli receptor FhuA. Biochimie 94:1982–1989. https://doi.org/10.1016/j.biochi.2012.05.021.
32. Breyton C, Flayhan A, Gabel F, Lethier M, Durand G, Boulanger P, Chami M, Ebel C. 2013. Assessing the conformational changes of pb5, the receptor-binding protein of phage T5, upon binding to its Escherichia coli receptor FhuA. J Biol Chem 288:30763–30772. https://doi.org/10.1074/jbc.M113.501536.
33. Locher KP, Rees B, Koebnik R, Mitschler A, Moulinier L, Rosenbusch JP, Moras D. 1998. Transmembrane signaling across the ligand-gated FhuA receptor: crystal structures of free and ferrichrome-bound states reveal allosteric changes. Cell 95:771–778. https://doi.org/10.1016/s0092-8674(00)81700-6.
34. Breyton C, Javed W, Vermot A, Arnaud C-A, Hajjar C, Dupuy J, Petit-Hartlein I, Le Roy A, Martel A, Thépaut M, Orelle C, Jault J-M, Fieschi F, Porcar L, Ebel C. 2019. Assemblies of lauryl maltose neopentyl glycol (LMNG) and LMNG-solubilized membrane proteins. Biochim Biophys Acta Biomembr 1861:939–957. https://doi.org/10.1016/j.bbamem.2019.02.003.
35. Flayhan A. 2012. Reconnaissance phage – bactérie dans le système phage T5 – *E. coli*. Caractérisation des premières étapes de l'infection. Thèse de Doctortat - Université Paris Diderot. https://www.theses.fr/2012PA077164.
36. Engilberge S, Riobé F, Pietro SD, Lassalle L, Coquelle N, Arnaud C-A, Pitrat D, Mulatier J-C, Madern D, Breyton C, Maury O, Girard E. 2017. Crystallophore: a versatile lanthanide complex for protein crystallography combining nucleating effects, phasing properties, and luminescence. Chem Sci 8:5909–5917. https://doi.org/10.1039/c7sc00758b.
37. Kühlbrandt W. 2014. Biochemistry. The resolution revolution. Science 343:1443–1444. https://doi.org/10.1126/science.1251652.
38. Pawelek PD, Croteau N, Ng-Thow-Hing C, Khursigara CM, Moiseeva N, Allaire M, Coulton JW. 2006. Structure of TonB in complex with FhuA, E. coli outer membrane receptor. Science 312:1399–1402. https://doi.org/10.1126/science.1128057.
39. Holm L. 2020. DALI and the persistence of protein shape. Protein Sci 29:128–140. https://doi.org/10.1002/pro.3749.
40. Garcia-Doval C, van Raaij MJ. 2012. Structure of the receptor-binding carboxy-terminal domain of bacteriophage T7 tail fibers. Proc Natl Acad Sci U S A 109:9390–9395. https://doi.org/10.1073/pnas.1119719109.
41. Cardarelli L, Pell LG, Neudecker P, Pirani N, Liu A, Baker LA, Rubinstein JL, Maxwell KL, Davidson AR. 2010. Phages have adapted the same protein fold to fulfill multiple functions in virion assembly. Proc Natl Acad Sci U S A 107:14384–14389. https://doi.org/10.1073/pnas.1005822107.
42. Alexander LT, Lepore R, Kryshtafovych A, Adamopoulos A, Alahuhta M, Arvin AM, Bomble YJ, Böttcher B, Breyton C, Chiarini V, Chinnam NB, Chiu W, Fidelis K, Grinter R, Gupta GD, Hartmann MD, Hayes CS, Heidebrecht T, Ilari A, Joachimiak A, Kim Y, Linares R, Lovering AL, Lunin VV, Lupas AN, Makbul C, Michalska K, Moult J, Mukherjee PK, Nutt WS, Oliver SL, Perrakis A, Stols L, Tainer JA, Topf M, Tsutakawa SE, Valdivia-Delgado M, Schwede T. 2021. Target highlights in CASP14: analysis of models by structure providers. Proteins 89:1647–1672. https://doi.org/10.1002/prot.26247.
43. Jumper J, Evans R, Pritzel A, Green T, Figurnov M, Ronneberger O, Tunyasuvunakool K, Bates R, Žídek A, Potapenko A, Bridgland A, Meyer C, Kohl SAA, Ballard AJ, Cowie A, Romera-Paredes B, Nikolov S, Jain R, Adler J, Back T, Petersen S, Reiman D, Clancy E, Zielinski M, Steinegger M, Pacholska M, Berghammer T, Bodenstein S, Silver D, Vinyals O, Senior AW, Kavukcuoglu K, Kohli P, Hassabis D. 2021. Highly accurate protein structure prediction with AlphaFold. Nature 596:583–589. https://doi.org/10.1038/s41586-021-03819-2.
44. Tunyasuvunakool K, Adler J, Wu Z, Green T, Zielinski M, Žídek A, Bridgland A, Cowie A, Meyer C, Laydon A, Velankar S, Kleywegt GJ, Bateman A, Evans R, Pritzel A, Figurnov M, Ronneberger O, Bates R, Kohl SAA, Potapenko A, Ballard AJ, Romera-Paredes B, Nikolov S, Jain R, Clancy E, Reiman D, Petersen S, Senior AW, Kavukcuoglu K, Birney E, Kohli P, Jumper J, Hassabis D. 2021. Highly accurate protein structure prediction for the human proteome. Nature 596:590–596. https://doi.org/10.1038/s41586-021-03828-1.
45. Evans R, O'Neill M, Pritzel A, Antropova N, Senior A, Green T, Žídek A, Bates R, Blackwell S, Yim J, Ronneberger O, Bodenstein S, Zielinski M, Bridgland A, Potapenko A, Cowie A, Tunyasuvunakool K, Jain R, Clancy E, Kohli P, Jumper J, Hassabis D. 2022. Protein complex prediction with AlphaFold-Multimer. bioRxiv. https://doi.org/10.1101/2021.10.04.463034.
46. Ashkenazy H, Abadi S, Martz E, Chay O, Mayrose I, Pupko T, Ben-Tal N. 2016. ConSurf 2016: an improved methodology to estimate and visualize evolutionary conservation in macromolecules. Nucleic Acids Res 44:W344–W350. https://doi.org/10.1093/nar/gkw408.
47. de Jonge PA, Nobrega FL, Brouns SJJ, Dutilh BE. 2019. Molecular and evolutionary determinants of bacteriophage host range. Trends Microbiol 27:51–63. https://doi.org/10.1016/j.tim.2018.08.006.
48. Krissinel E, Henrick K. 2004. Secondary-structure matching (SSM), a new tool for fast protein structure alignment in three dimensions. Acta Crystallogr D Biol Crystallogr 60:2256–2268. https://doi.org/10.1107/S0907444904026460.
49. Mondigler M, Holz T, Heller KJ. 1996. Identification of the receptor-binding regions of pb5 proteins of bacteriophages T5 and BF23. Virology 219:19–28. https://doi.org/10.1006/viro.1996.0218.
50. Killmann H, Videnov G, Jung G, Schwarz H, Braun V. 1995. Identification of receptor binding sites by competitive peptide mapping: phages T1, T5, and phi 80 and colicin M bind to the gating loop of FhuA. J Bacteriol 177:694–698. https://doi.org/10.1128/jb.177.3.694-698.1995.
51. Endriss F, Braun V. 2004. Loop deletions indicate regions important for FhuA transport and receptor functions in Escherichia coli. J Bacteriol 186:4818–4823. https://doi.org/10.1128/JB.186.14.4818-4823.2004.
52. Braun M, Endriss F, Killmann H, Braun V. 2003. In vivo reconstitution of the FhuA transport protein of Escherichia coli K-12. J Bacteriol 185:5508–5518. https://doi.org/10.1128/JB.185.18.5508-5518.2003.
53. Kandiah E, Giraud T, de Maria Antolinos A, Dobias F, Effantin G, Flot D, Hons M, Schoehn G, Susini J, Svensson O, Leonard GA, Mueller-Dieckmann C. 2019. CM01: a facility for cryo-electron microscopy at the European Synchrotron. Acta Crystallogr D Struct Biol 75:528–535. https://doi.org/10.1107/S2059798319006880.

54. Zivanov J, Nakane T, Forsberg BO, Kimanius D, Hagen WJ, Lindahl E, Scheres SH. 2018. New tools for automated high-resolution cryo-EM structure determination in RELION-3. Elife 7:e42166. https://doi.org/10.7554/eLife.42166.
55. Zheng W, Wang F, Taylor NMI, Guerrero-Ferreira RC, Leiman PG, Egelman EH. 2017. Refined cryo-EM structure of the T4 tail tube: exploring the lowest dose limit. Structure 25:1436–1441.e2. https://doi.org/10.1016/j.str.2017.06.017.
56. Zhang K. 2016. Gctf: real-time CTF determination and correction. J Struct Biol 193:1–12. https://doi.org/10.1016/j.jsb.2015.11.003.
57. Sanchez-Garcia R, Gomez-Blanco J, Cuervo A, Carazo JM, Sorzano COS, Vargas J. 2021. DeepEMhancer: a deep learning solution for cryo-EM volume post-processing. Commun Biol 4:874. https://doi.org/10.1038/s42003-021-02399-1.
58. Morin A, Eisenbraun B, Key J, Sanschagrin PC, Timony MA, Ottaviano M, Sliz P. 2013. Collaboration gets the most out of software. Elife 2:e01456. https://doi.org/10.7554/eLife.01456.
59. Mirdita M, Schütze K, Moriwaki Y, Heo L, Ovchinnikov S, Steinegger M. 2022. ColabFold: making protein folding accessible to all. Nat Methods 19:679–682. https://doi.org/10.1038/s41592-022-01488-1.

Supplemental Material for

Deciphering bacteriophage T5 host recognition mechanism and infection trigger

Structure of phage T5 RBP bound to its receptor

Séraphine Degroux[$a], Grégory Effantin[$a], Romain Linares[a], Guy Schoehn[a] and

Cécile Breyton[a#]

[a]Univ. Grenoble Alpes, CNRS, CEA, IBS, F-38000, Grenoble, France.

[$]These authors contributed equally to the work
#Corresponding author's email: Cecile.Breyton@ibs.fr.

Keywords: Bacteriophage, electron cryo-microscopy, host recognition, conformational changes

Figure S1 and S2

Table S1

PBD file of AF-RBP_{pb5} in a separate file

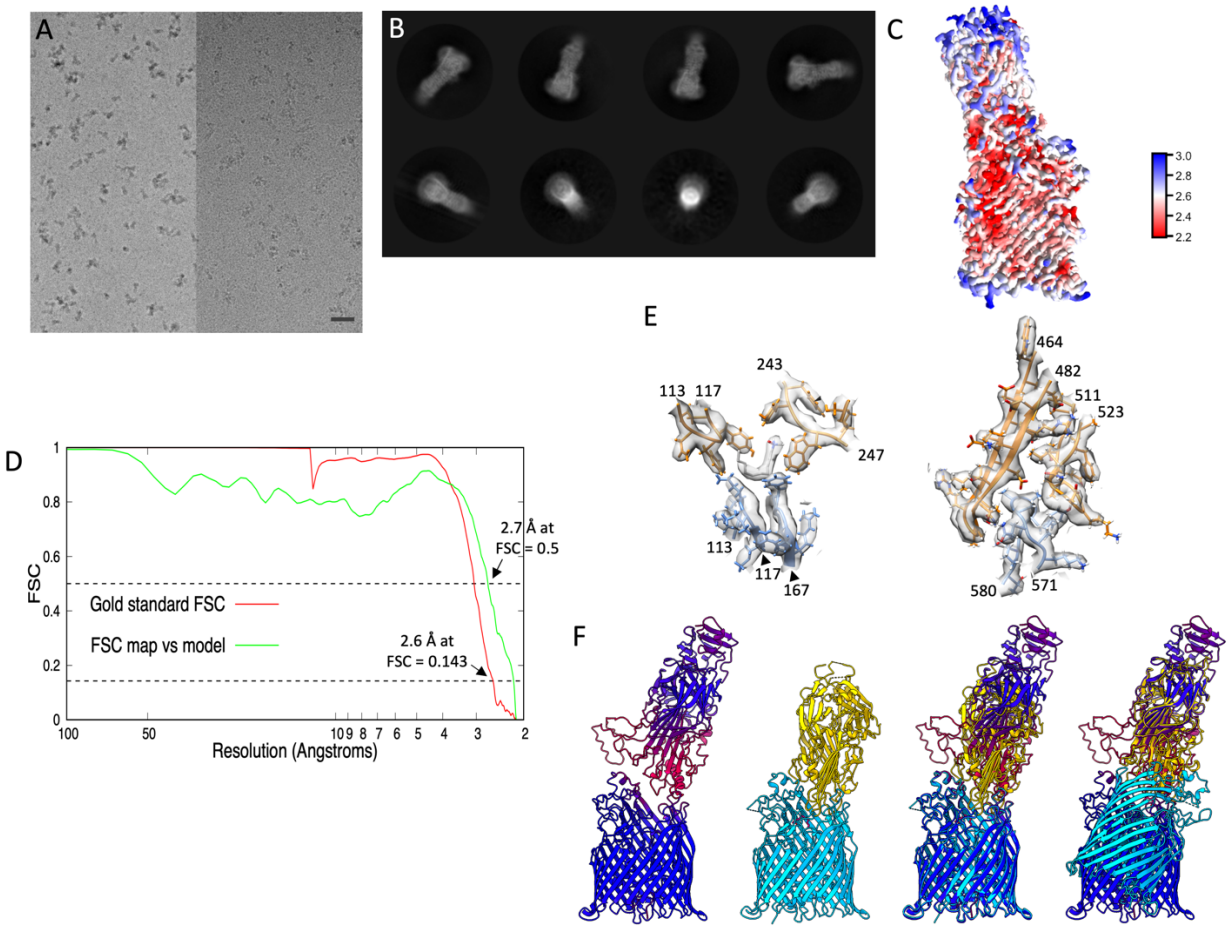

Figure S1: A. Cryo-EM field of views of FhuA-RBP$_{pb5}$ molecules with (left) and without (right) phase plate. Scale bar: 30 nm. **B.** Exemplary 2D class averages of FhuA-RBP$_{pb5}$ obtained from the dataset without phase plate. **C.** Local resolution map of the 3D reconstruction of FhuA-RBP$_{pb5}$ obtained with the dataset without phase plate. **D.** Fourier Shell Correlation (FSC) curves: gold standard FSC between two independent 3D reconstructions of FhuA- RBP$_{pb5}$ (red) and FSC between the cryo-EM coulomb potential map and the refined atomic model (green). The two dotted horizontal lines represent FSC = 0.143 and 0.5 which are used as cutoffs to determine the resolutions between the two different sets of maps. **E.** Illustrations of the quality of the obtained 3D reconstruction and atomic model. The coulomb potential map is in transparent gray while FhuA, RBP$_{pb5}$ and C_{10}DAO are colored, orange, blue and grey respectively. The left panel is centered around the interaction of FhuA and RBP$_{pb5}$ with C_{10}DAO while the right panel represents one of the interacting areas between FhuA and RBP$_{pb5}$ centered around loop 571-580 of RBP$_{pb5}$. **F.** From left to right: AF2-FhuA-RBP$_{pb5}$ best prediction, coloured by prediction confidence score (high pLDDT: blue, low pLDDT: dark magenta), cryo-EM FhuA-RBP$_{pb5}$ structure (FhuA: cyan, RBP$_{pb5}$: gold), alignment of AF2-FhuA-RBP$_{pb5}$ on FhuA and on RBP$_{pb5}$ of the cryo-EM structure.

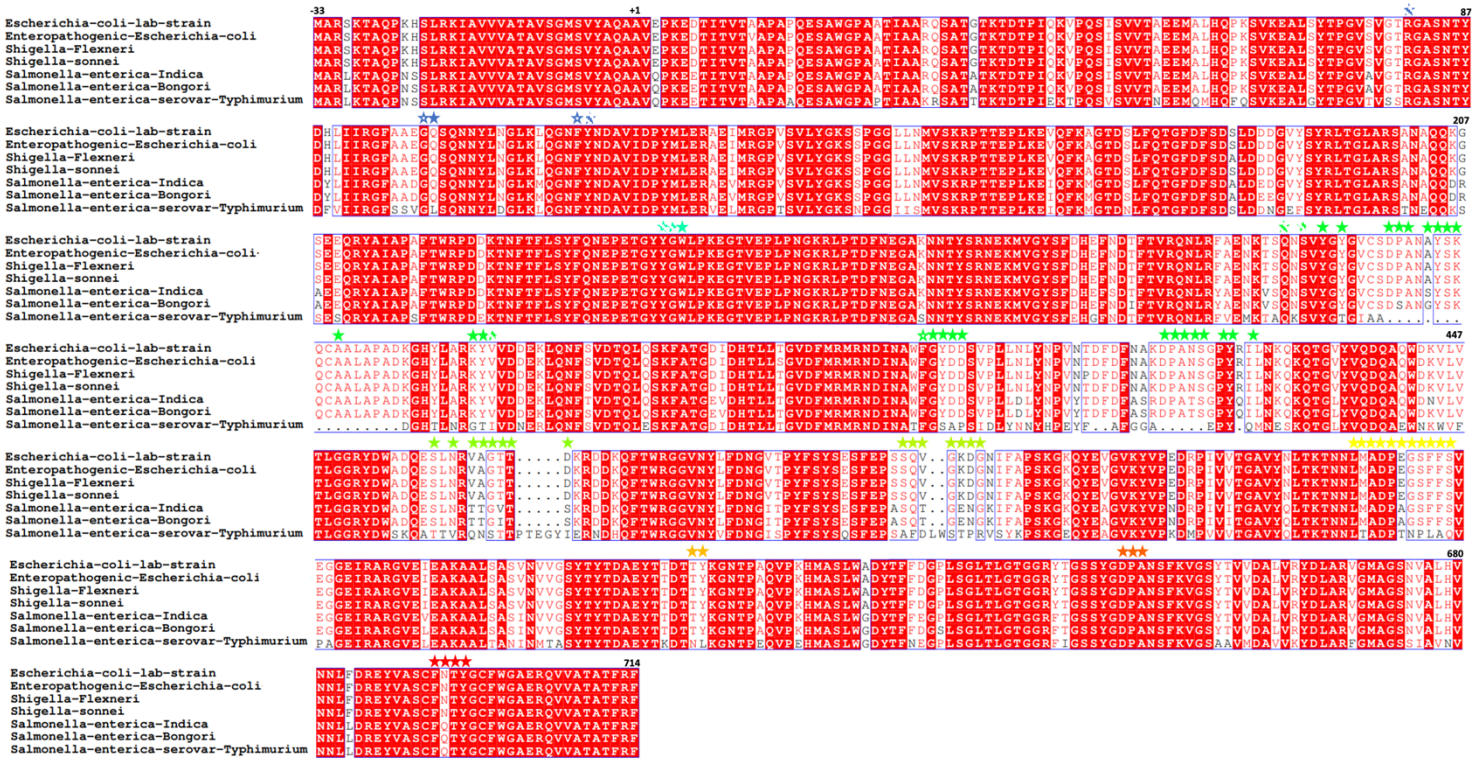

Figure S2 : Sequence alignment of FhuA in *E.coli*, *Shigella* and *Salmonella* strains. The alignment was performed with Clustal Omega (https://www.ebi.ac.uk/Tools/msa/clustalo/) and visualised with ESPript (https://espript.ibcp.fr/ESPript/ESPript/). Conserved residues are highlighted in red. Stars show residues involved in the FhuA-RBP_{pb5} interaction. Residues interacting exclusively with RBP_{pb5} (full), with both C_{10}DAO and RBP_{pb5} (empty) or with C_{10}DAO only (hatched) are coloured with the same colour code as in Figure 4. Note that the 9 residues of FhuA His-tag are not included in the alignment nor in the numbering.

Table S1: Summary of data collection and atomic model statistics

Data collection	
Microscope	Titan Krios G3
Voltage (kV)	300
Magnification Unbinned pixel size	130,000 x 1.052 Å/pixel
Camera	K2 Summit (Gatan Inc)
Exposure time	8 s
Number of frames	60
Total dose ($e^-/Å^2$)	60
Image processing	
EMDB	
Rotational symmetry	C1
Final number of Particles	109,350
Average map resolution in Å (FSC 0.143)	2.6
PDB	
Map to Model resolution in Å (FSC 0.5)	2.7
Ramachandran favoured (%)	97.2
Ramachandran outliers (%)	0.0
Rama Z score	0.3
Rotamer outliers (%)	0.8
C-beta deviations	0
Rms on bond lengths	0.0072
Rms on bond angles	1.05
Clashscore	7.1
Molprobity score	1.53